

Supplement of Atmos. Meas. Tech., 13, 2413–2423, 2020
<https://doi.org/10.5194/amt-13-2413-2020-supplement>
© Author(s) 2020. This work is distributed under
the Creative Commons Attribution 4.0 License.



Supplement of

Laboratory evaluation of particle-size selectivity of optical low-cost particulate matter sensors

Joel Kuula et al.

Correspondence to: Joel Kuula (joel.kuula@fmi.fi)

The copyright of individual parts of the supplement might differ from the CC BY 4.0 License.

Supplemental Table S1. Running parameters of the VOAG and GP50.

Parameter	Value
Dilution air flow rate	20 L min ⁻¹
Dispersion air flow rate	1.5 L min ⁻¹
Liquid feed rate	0.12 mL min ⁻¹
Disturbance frequency	45 kHz
VOAG orifice diameter	20 μm
2-Propanol impurity	< 1 ppm
DOS concentration A	9.14 g L ⁻¹ in 2-propanol (1:100)
DOS concentration B	0.609 g L ⁻¹ in 2-propanol (1:1,500)
DOS concentration C	0.0914 g L ⁻¹ in 2-propanol (1:10,000)
DOS concentration D	Pure 2-propanol

Supplemental Table S2. Running steps and respective blending ratios of the GP50 dispensing program. Use of three eluent channels was sufficient for this study.

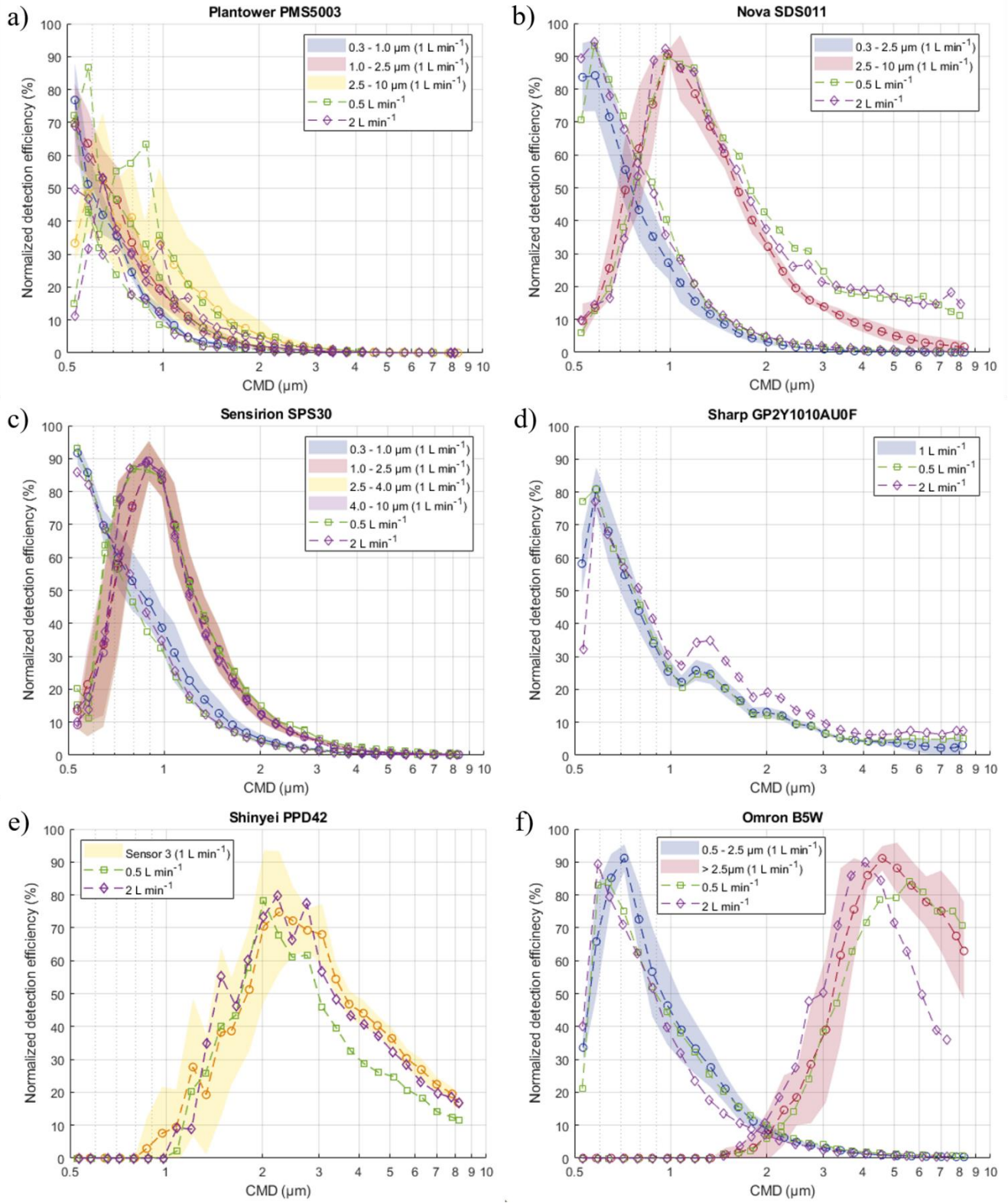
Step	Channel A	Channel B	Channel C	Elapsed time (min)	Particle size (μm)
1	0.00	0.00	1.00	0	0.45
2	0.00	0.02	0.98	5	0.63
3	0.00	0.07	0.93	10	0.89
4	0.00	0.22	0.78	15	1.25
5	0.00	0.63	0.37	20	1.76
6	0.02	0.00	0.98	25	2.48
7	0.05	0.00	0.95	30	3.49
8	0.14	0.00	0.86	35	4.91
9	0.39	0.00	0.61	40	6.92
10	1.00	0.00	0.00	45	9.73



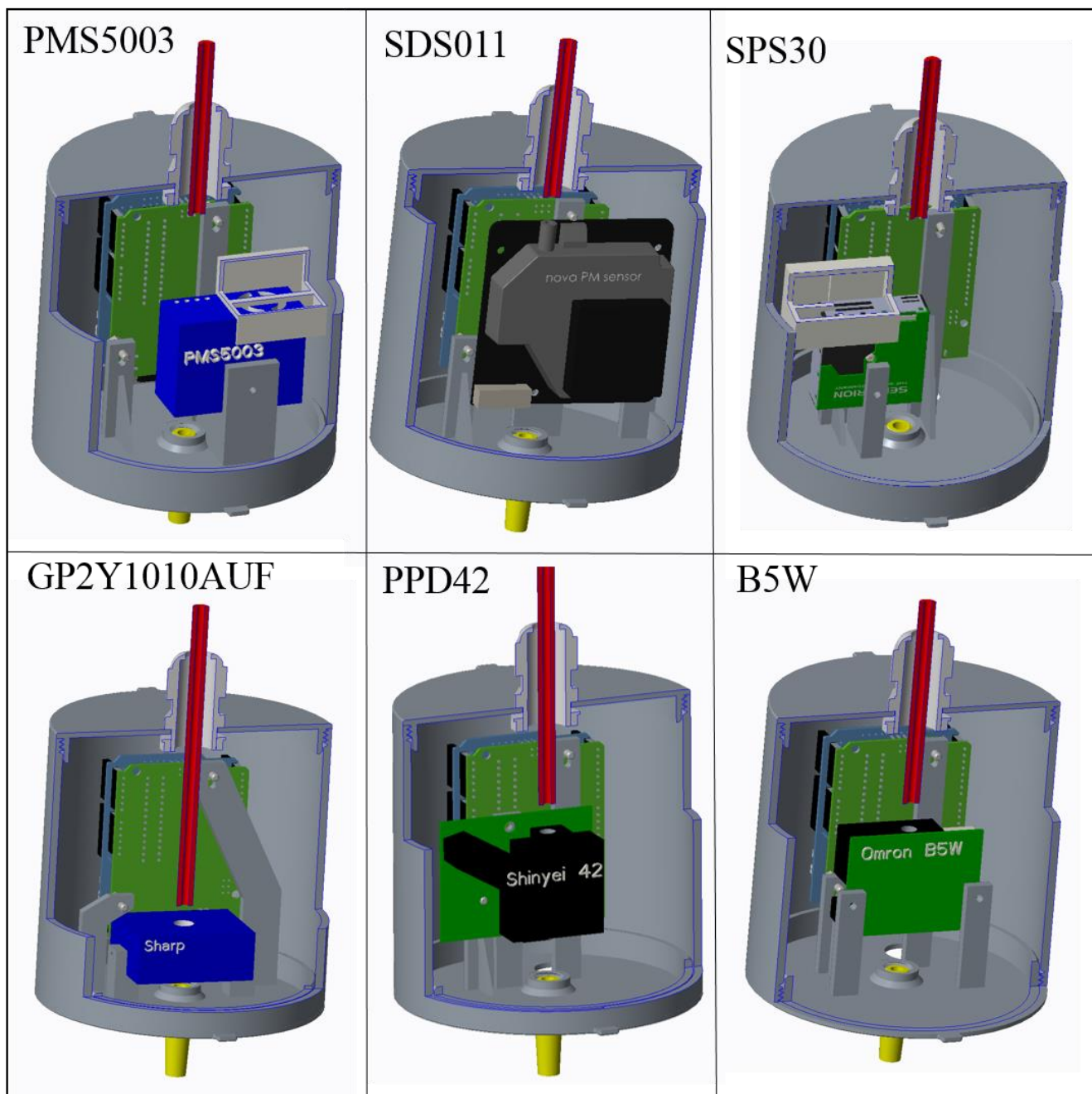
Supplemental Figure S1. Optical detection configurations. The dashed red arrow points out the particle stream pathway.

Additional tests with flow rates of 0.5 and 2 L min⁻¹

To ensure that the ancillary flow rate did not affect the results, additional tests were conducted with flow rates of 0.5 and 2 L min⁻¹. A single sensor unit (unit #3) was evaluated and the test runs were conducted once for each flow rate. The results (Figure S2) indicate that different flow rates had no meaningful effect on the sensor responses. The SDS011 shows slightly stronger response for particles larger than ~2 – 3 μm, but this is probably resulting from operator inconsistency (or randomness) because the change is similar for both 0.5 and 2 L min⁻¹ flow rates. The B5W sensor has weaker response for particle sizes larger than ~4 – 5 μm with 2 L min⁻¹ flow rate which suggests that the sampling losses may have increased. However, the response is similar for 0.5 and 1 L min⁻¹ flow rates (B5W was originally designed to be used with a heater resistor-induced flow which is most probably closer to 0.5 than 2 L min⁻¹). The difference in PPD42NS responses, which imply that the losses may have increased for smaller and not higher flow rates, is attributed to randomness. The Sharp GP2Y1010AU0F sensors appear to be affected by different flow rates in smallest particle sizes (< 0.55 μm), but the responses with 0.5 and 1 L min⁻¹ flow rates are so similar that the stated valid detection range remains the same. Smaller flow rates are likely to better represent the original flow rate, which for the Sharp sensors, was based on plain diffusion.



Supplemental Figure S2. The effect of different ancillary flow rates.

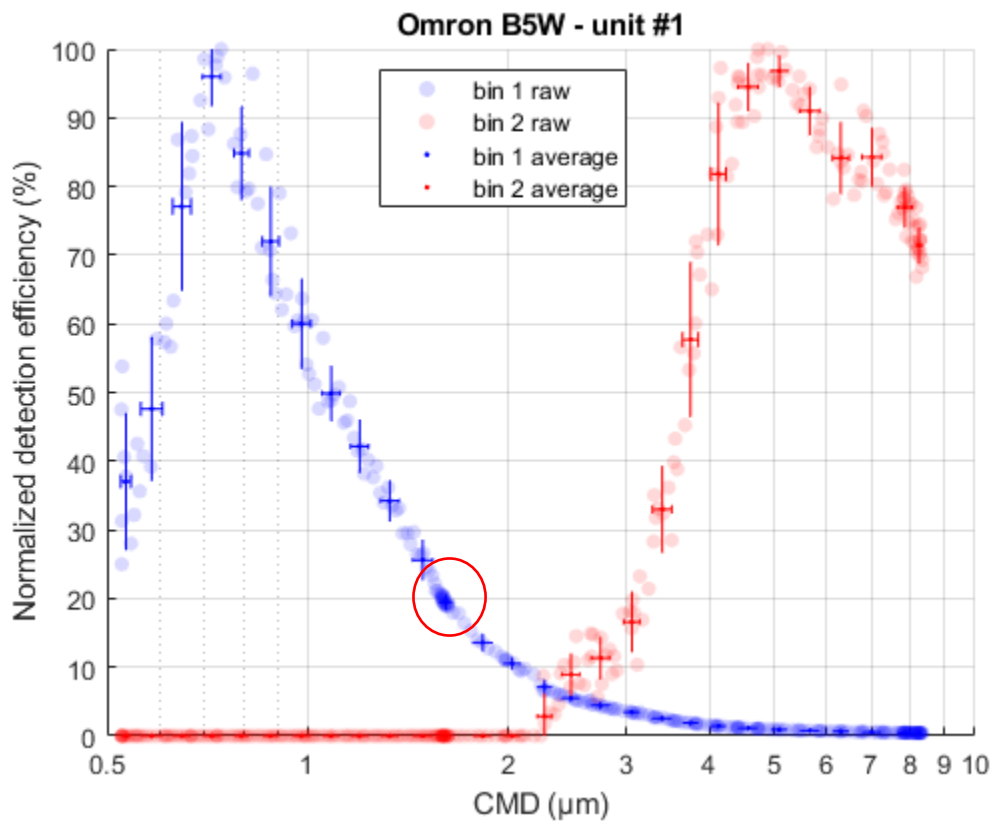


Supplemental Figure S3. A cross-section view of the used inlet arrangements. The inlet pipe of the air-tight enclosure is colored red and the outlet connector, which was attached to the external pump, is colored yellow. The exhaust flow deflectors (also viewed as cross-sections) of the PMS5003 and SPS30 are shown as light grey in their respective figure panels. Data logging hardware was positioned behind the sensor.

Detailed description of the data processing method used

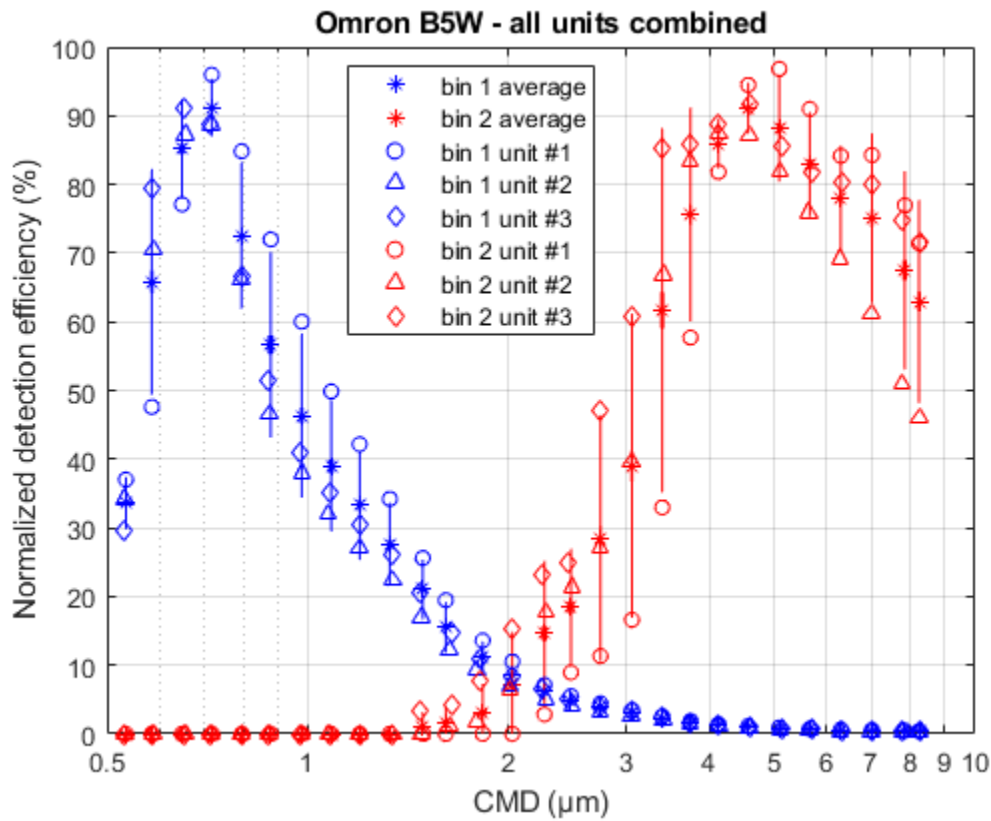
Supplemental Figure S4 shows the normalized and filtered (data points with GSD greater than 1.2 removed) 10-second resolution data of the Omron B5W unit #1 test. Raw data is plotted as transparent bullets and the average values and respective standard deviations (for both CMD and normalized detection efficiency) as solid dots. The raw data was divided into 30 different sections which were logarithmically spaced to 0.45 – 9.73 μm range. This range was the theoretical size range of the produced particles. In the figure, each section corresponds to each solid dot (blue and red), and in this case, a total of 28 dots (for each color) are visible. This is because in practice the first and last section (0.45 – 0.50 and 8.80 – 9.73 μm) did not contain any measurement points.

Despite shown here, the standard deviations of the raw data were not utilized in any form as the final statistical uncertainties were calculated from the average responses of the three individual units. By using the “average of averages”, all units had an equal contribution to the final statistics (28 data points each) as in some occasions, the total number of raw data points and the way the points were spaced along different particle sizes varied. See for example the red circle in Fig. S4; for an unknown reason, the speed at which the particle size gradient was evolving decreased momentarily and thus resulted in a cluster of data points. If the raw data would have been used as such, the cluster would have distorted the calculations of average due to the greater number of data points at this specific particle size.

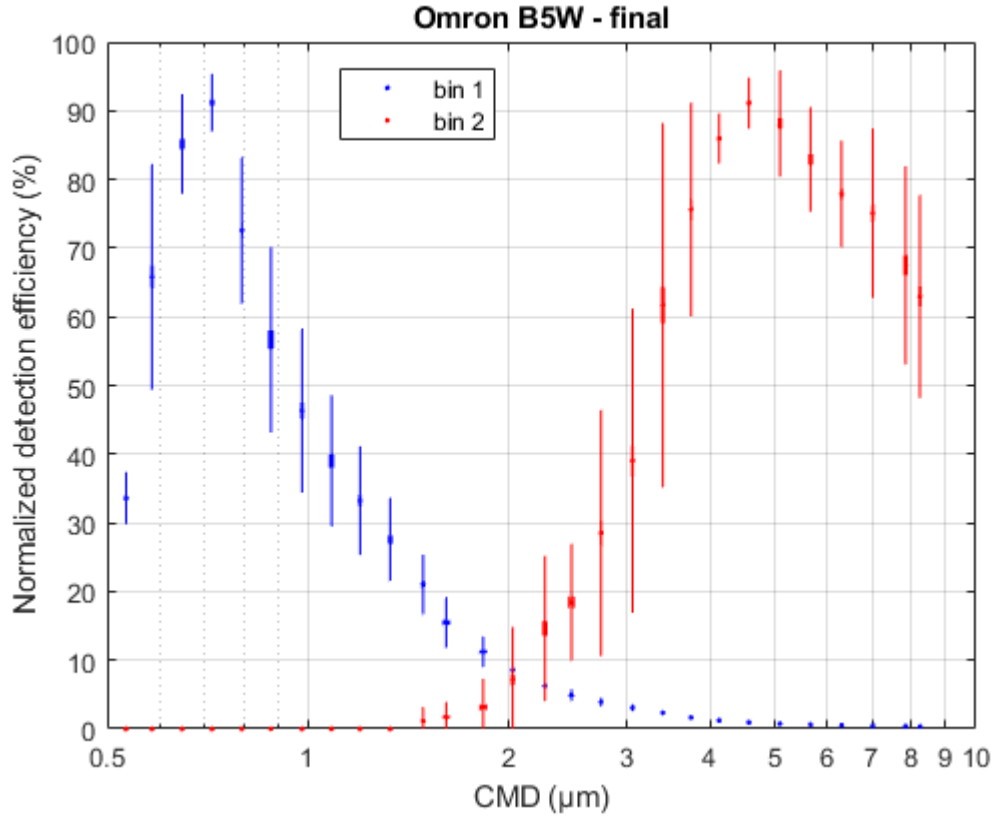


Supplemental Figure S4. Normalized and filtered (GSDs greater than 1.2 removed) data of the Omron B5W unit #1 test run. The raw 10-sec resolution data is shown as transparent bullets and the calculated average values of the 30 different size sections as solid dots (with standard deviations).

The average responses of the three Omron B5W units are shown in Supplemental Figure S5. The circle, triangle, and diamond markers stand for the average responses of the individual units #1, #2, and #3, respectively, and “the average of the averages” (and respective standard deviations) are shown in the figure as star markers. The standard deviations of the average CMDs are negligible compared to the differences observed in normalized detection efficiencies and thus they were not shown in the final manuscript Figure 4f. Supplemental Figure S6, which is essentially the same figure as the final manuscript Figure 4f but with standard deviations of the CMDs included, shows again the insignificance of the CMD standard deviations.



Supplemental Figure S5. Averaged responses of the three individual sensor units.



Supplemental Figure S6. Final normalized detection efficiency of the Omron B5W (with standard deviations).

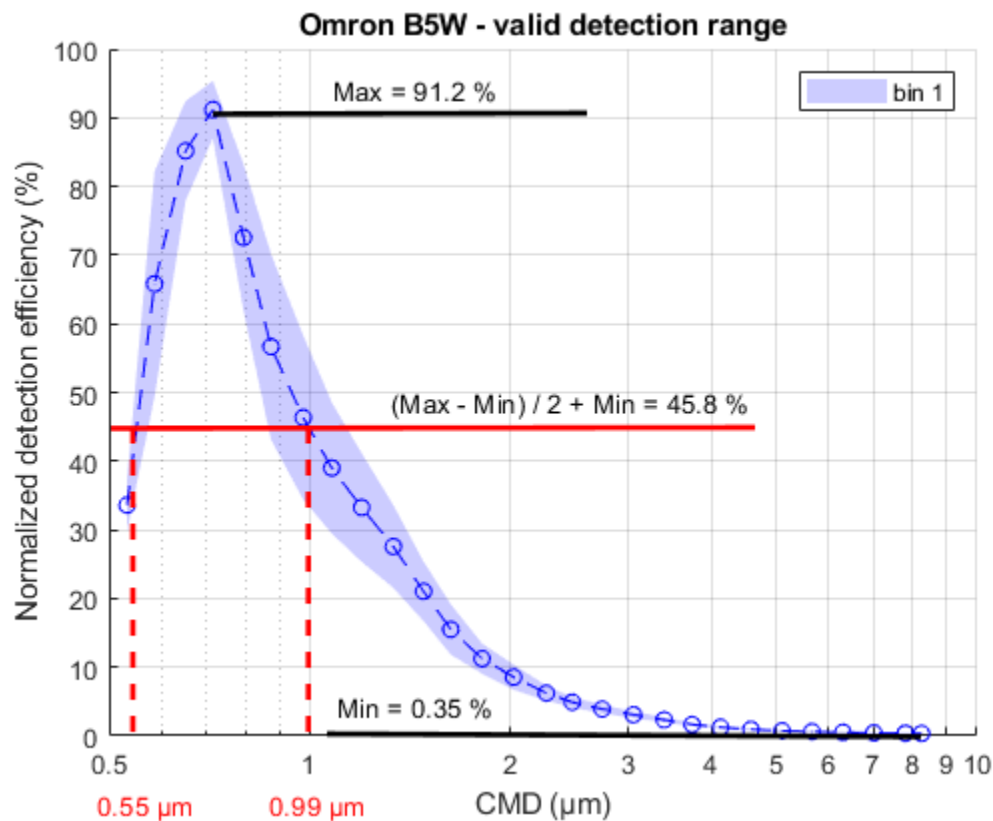
Definition of the valid detection range

In order to interpret the normalized detection efficiency curves, a concept of valid detection range was used. Valid detection range refers to the particle size range which the sensor is most capable measuring of. It is a similar concept to the commonly used “lower” and “upper cut-points” which are typically defined as the particle size points where the device counts 50 % of the total number of particles. In this study, however, a value of 50 % normalized detection efficiency was not used as a threshold as the normalized detection efficiency does not describe what percentage of the absolute concentration was measured and the obtained normalized detection efficiency ranges were not the same for every sensor model (i.e. from 0 to 100 %). Instead, the valid detection ranges were defined as particle size ranges where the normalized detection efficiency was greater than 50 % (greater than half) of the total measured detection efficiency range. The threshold value defining the limit for the size range “greater than 50 %” is shown in Eq. S1:

$$\text{Valid detection range threshold} = \frac{\max(NDE) - \min(NDE)}{2} + \min(NDE) \quad (S1)$$

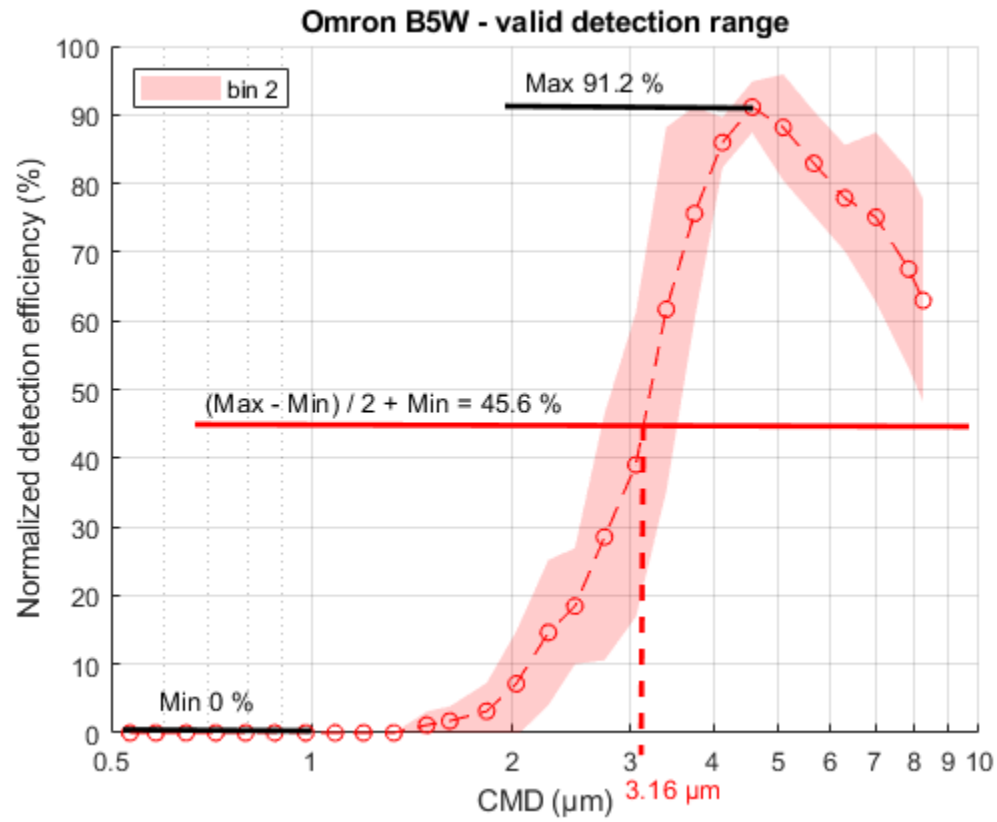
Where NDE stands for normalized detection efficiency.

Supplemental Figure S7 illustrates how the valid detection range of the Omron B5W sensor was calculated. The minimum and maximum detection efficiencies were measured to be 0.35 and 91.2 %, respectively, and thus, the mid-point (or threshold) of this range is 45.8 %. By linearly interpolating the normalized detection efficiency curve, the valid detection range (or the upper and lower cut-points), can be calculated. Rounding the interpolated values to two significant decimals yields a valid detection range of 0.6 – 1.0 μm for the bin 1 of the Omron B5W.



Supplemental Figure S7. Valid detection range (0.55 – 0.99 μm) of the Omron B5W bin 1.

In cases where either the lower or the upper cut-point fell outside the calculated threshold, a symbol of “greater than” or “smaller than” was used to denote the valid detection range. An example of this is shown Supplemental Figure S8, where the valid detection range of the Omron B5W bin 2 has been calculated. The lower cut-point is shown to be 3.16 μm but the upper cut-point falls outside the particle size range to which the sensor response was compared. Thus, by rounding the lower cut-point to two significant decimals, the valid detection range of the bin 2 is stated to be > 3.2 μm .



Supplemental Figure S8. Valid detection range (> 3.16 μm) of the Omron B5W bin 2.